CHARACTERISTICS OF TROPICAL CYCLONE GENESIS FORECASTS AND UNDERDISPERSION IN HIGH-RESOLUTION ENSEMBLE FORECASTING WITH A STOCHASTIC KINETIC ENERGY BACKSCATTER SCHEME

Levi Thatcher and Zhaoxia Pu*

Department of Atmospheric Sciences, University of Utah, Salt Lake City, Utah, USA

ABSTRACT

This study evaluates ensemble forecasts with a stochastic kinetic energy backscatter scheme (SKEBS) to predict tropical cyclone (TC) genesis and also to characterize the related ensemble underdispersion. Several sets of ensemble forecasts are generated using an advanced research version of the Weather Research and Forecasting model at 5 km horizontal resolution to predict the genesis of Hurricane Ernesto (2006) and Typhoon Nuri (2008). Ensemble forecasts with SKEBS are compared against a control ensemble forecast with the WRF model using downscaled initial conditions derived from the NCEP Global Ensemble Forecasting System.

It is found that ensemble forecasts with SKEBS are able to generate probabilistic forecasts for TC genesis and also capable of indicating the forecast uncertainties. Compared with the deterministic forecast that fails to predict the genesis of Typhoon Nuri, the ensemble forecast with SKEBS is able to produce the genesis forecast. However, the underdispersion of ensemble forecasts with SKEBS is also present in all cases in terms of the simulation period and over the whole model domain, TC environment, and inner core regions, although it is reduced near the TC inner core region. In addition, the initial perturbation–based ensemble forecasts shows slightly less underdispersion compared with the SKEBS ensembles.

Keywords: tropical cyclone genesis, stochastic kinetic energy backscatter, ensemble forecasting, WRF

1. Introduction

Owing to increases in computing power and the development of sophisticated perturbation techniques, the use of ensemble forecasts in numerical weather prediction (NWP) has grown substantially over the last several decades. The primary benefits of these ensembles above and beyond standard deterministic forecasts are twofold: 1) if properly constructed, the ensemble forecast provides a better forecast of the mean and 2) the ensemble forecast provides an estimate of the associated forecast uncertainty.

Overall, ensemble forecasts have focused on accounting for 1) the uncertainty in the initial conditions and 2) the error associated with the model itself. In the past two decades, many operational centers have implemented ensemble forecasts that deal with initial condition errors (Toth and Kalnay 1993, 1997; Buizza 1997; Wei et al. 2006). Ensemble forecasts accounting for model errors have also been implemented in some operational centers. But, our knowledge about how to address model errors is still limited (Reynolds et al. 2008). Typically, model errors come from the associated dynamic core because of the use of the discretization numerical scheme, the numerical method to calculate advection term, and related truncation error (Shutts 2005). In addition, parameterizations of subgrid-scale processes contribute significantly to model errors (Teixeira and Reynolds 2008).

Various ensemble methods have been created to account for the presence of model errors. For instance, multimodel ensemble forecasts are used to mitigate the idiosyncrasies associated with one particular model (Hagedorn et al. 2005). Fritsch et al. (2000) concluded that "variations in model physics and numerics play a substantial role in generating the full spectrum of possible solutions." In addition, some researchers have used different parameterization schemes within a single model to achieve multiphysics ensemble forecasts (Houtekamer et al. 1996). Others have developed formulations that impose a stochastic term onto the physical parameterizations (Teixeira and Reynolds 2008).

While large attention has been given to errors related to physical parameterizations (e.g., Teixeira and Reynolds 2008), the errors due to numerical schemes (or the dynamic core) and their interactions with physical parameterization

Corresponding author address: Dr. Zhaoxia Pu, Department of Atmospheric Sciences, University of Utah, 135 S 1460 E, Rm. 819, Salt Lake City, UT 84112. E-mail: Zhaoxia.Pu@utah.edu.

DOI: 10.6057/2014TCRR04.01

has not been accounted until recent studies have focused on measuring a little-studied but unrealistically large energy sink, which is due primarily to numerical advection error and horizontal diffusion (Shutts 2005). Berner et al. (2009) indicated that model simulations do not produce the observed $n^{-5/3}$ inertial-range power spectrum below 400 km wavelengths as found by Nastrom and Gage (1985). Shutts (2005) argued that routine kinetic energy loss is an underlying problem in both numerical integration schemes and parameterizations. He asserted "a suitably contrived near-grid-scale stochastic forcing function could be used to inject energy back into the model." Then, he implemented the first backscatter scheme into an NWP model. Specifically, he used a cellular automaton (CA) to generate evolving patterns, along with a dissipation function, to ultimately define a streamfunction forcing field that directly affected the model dynamics (Shutts 2005). His CA method represented largely temporal and spatial correlations for the mesoscale atmosphere. The CA pattern, after being scaled by the square root of the dissipation rate, is proportional to the streamfunction forcing.

Fundamentally, the stochastic kinetic energy backscatter scheme (SKEBS) introduced by Shutts (2005) addresses a missing dynamical process in a model through a two-way exchange of kinetic energy across the model truncation boundary. In other words, the backscatter scheme adds "perturbations that mimic the influence of altogether unrepresented subgrid-scale processes" (Berner et al. 2009) into the numerical model. This is physically important, as the excessive model energy dissipation inhibits part of the turbulent inverse cascade. The lack of this simulated inverse cascade could contribute to an error tendency on the order of 5 m s^{-1} per day in terms of horizontal winds (Shutts 2005; Charron et al. 2010). SKEBS attempts to counter not only kinetic-energy dissipation due to advection and diffusion, but also that due to parameterized mountain drag and deep convection. By countering the total dissipation rate with his SKEBS, Shutts (2005) found that the ECMWF model consequently benefited in terms of probabilistic measures of forecast skill. The method also corrected the previously-too-steep spectral slope in kinetic energy spectra, thus moving it toward the $k^{-5/3}$ rate typically found in mesoscale observations.

Charron et al. (2010) evaluated a SKEBS method (see Li et al. 2008) that was similar to that of Shutts (2005) and implemented it at the Meteorological Service of Canada. When using the backscatter scheme in their newly redesigned model, they found notably large biases in the low-level temperature field (Charron et al. 2010). They admitted that the physical mechanism behind these biases was not clear, but overall, the backscatter scheme helped improve forecast reliability primarily by improving ensemble dispersion, especially zonal winds at 850 hPa and geopotential height at 500 hPa.

Instead of using a CA as Shutts (2005) did, Berner et al. (2009) used a first-order autoregressive process on each spherical harmonic of the streamfunction forcing to control spatial and temporal correlations and also the spectral characteristics of the perturbations. In addition, they also used cloud-resolving models to inform parameters of the backscatter scheme regarding the "power-law exponent of the forcing streamfunction" (Berner et al. 2009). By implementing such a method in the ECMWF ensemble prediction system, they achieved a better spread-error relationship, improved rainfall forecasts, and provided better probabilistic skill compared to simulations without the backscatter scheme.

Following the success with global models, Berner et al. (2011) adapted the method to a mesoscale community model, namely, an advanced research version of the Weather Research and Forecasting (WRF) model (Skamarock et al. 2008). To convert the backscatter scheme from the pseudospectral-core global ECMWF system to a limited-area WRF model that uses finite difference schemes, they changed the basic functions of the SKEBS "from spherical harmonics to 2D-Fourier modes" (Berner et al. 2011). By comparing the scheme to ensemble experiments with both 1) various physics parameterizations and 2) a combination of the backscatter scheme combined with the multiphysics, they found that the stochastic backscatter scheme outperformed the ensemble using multiple combinations of different physics schemes. In general, however, the best-performing ensemble was the one that combined the multiphysics scheme with the stochastic energy backscatter scheme.

While the backscatter scheme has generally helped reduce ensemble underdispersiveness, a number of unresolved issues remain. First, even with the help of SKEBS, studies (Shutts 2005; Berner et al. 2009) have not been able to effectively replicate the $k^{-5/3}$ spectral slope that is found in the observations of Nastrom and Gage (1985). In addition, much of the research into the various SKEBS implementations has examined ensemble forecasts with horizontal grid spacing generally at or above 45 km (Shutts 2005; Charron et al. 2010; Berner et al. 2011). Studies using SKEBS at higher resolutions (less than 10 km horizontal grid spacing) have been quite rare.

At higher resolutions, the model has less dependence on physics parameterizations than at coarser resolutions. This somewhat inhibits the kinetic-energy spectral drop-off at smaller scales. However, because of the numerical computational methods used to solve the NWP equations and also because the physical parameterizations are still needed, these mesoscale models may still suffer the same energy-dissipation issues.

Consequently, the ability of backscatter schemes to increase dispersion in high-resolution models has been largely neglected in the literature. Ideally, the spread among the ensemble members matches the error inherent in the forecast. Partially because of model error, however, ensembles

are generally underdispersive (Berner et al. 2009), which means the members typically do not account for all the possibilities inherent in the forecast. As a result, ensemble spread will underestimate the uncertainties in the forecast and thus allow overconfidence in the forecast products. Elevated ensemble dispersiveness was indeed seen as being the most important beneficial component of the impact of SKEBS on forecast reliability (Charron et al. 2010). However, this benefit has not yet been examined in high-resolution ensemble forecasting, mainly because of the lack of operational high-resolution ensemble systems.

In order to examine the performance of SKEBS in high-resolution ensemble forecasts and also to characterize ensemble dispersion in the mesoscale, in this study we use WRF model version 3.4.1, with SKEBS implemented in the forecasts (Berner et al. 2011), to conduct a series of ensemble experiments to evaluate the underdispersion. Specifically, since the predictability of tropical cyclone (TC) genesis is a notable challenge in NWP and there have not yet been many high-resolution ensemble studies emphasizing this topic, we choose to examine the effect of SKEBS and characterize the underdispersion of ensemble forecasts in TC genesis environments. Hurricane Ernesto (2006) over the Atlantic Ocean and Typhoon Nuri (2008) over the western Pacific Ocean are used as case studies for reasons discussed below.

This paper is organized as follows: Section 2 describes the cases, model configuration, and design of the experiments; Section 3 evaluates the results from the various ensemble experiments with SKEBS in terms of bias, dispersion, and TC genesis forecasts; and Section 4 summarizes the major findings and discusses future work.

2. Description of the cases, WRF model, and ensemble forecasts

a. Hurricane Ernesto (2006)

Although originating as a tropical wave off the coast of Africa, Hurricane Ernesto (2006) did not achieve any notable organization until an associated surface low developed as the disturbance approached the Lesser Antilles. Moving toward the northeast, the disturbance developed as a tropical depression (TD) at 1800 UTC on 24 August 2006, roughly 40 nautical mi north-northwest of Grenada. Subsequently, the depression experienced increased convection over the low-level center as it moved north-northwest below a ridge over the western Atlantic Ocean. At 1200 UTC 25 August 2006, the disturbance reached tropical storm (TS) status and turned to the northwest. Later, at 0600 UTC 27 August, the storm reached hurricane status just south of Haiti. Then, Ernesto experienced several periods of strengthening and weakening and eventually made landfall in Cuba, Florida, and North Carolina, according to the report from the National Hurricane Center.

Hurricane Ernesto (2006) is chosen as the primary focus of this study because 1) it caused significant damage in the US and Caribbean and 2) it has been documented as an especially difficult forecast for the NCEP Global Ensemble Forecast System (GEFS) (Snyder et al. 2010; Liu et al. 2012).

b. Typhoon Nuri (2008)

Typhoon Nuri (2008) is also notoriously difficult to forecast using large-scale ensembles. Two days before genesis, Navy Operational Global Atmospheric Prediction System (NOGAPS) forecasts, conducted as part of the T-PARC/TCS-08 field campaigns, showed a highly uncertain forecast, as the 32 ensemble members predicted anything from full-fledged genesis to nondevelopment (Snyder et al. 2011).

Nuri originated from a "finite-amplitude wave/vortex structure" that tracked westward in the west Pacific several days before the disturbance reached tropical depression (TD) status, around 1800 UTC 16 Aug 2008, according to the Joint Typhoon Warning Center (JTWC).

c. WRF configuration

The WRF-ARW model (Skamarock 2008) Version 3.4.1 is used with three-level nested domains at 45 km, 15 km, and an innermost resolution of 5 km. Detailed information on the domain configurations is presented in Tables 1 and 2 for Hurricane Ernesto and Typhoon Nuri, respectively. The location of the domains is displayed in Figure 1. The top of the model is set at 50 hPa, and there are 36 vertical σ levels. The Purdue Lin (Chen and Sun 2002) scheme is used for the microphysics, the Yonsei University scheme (Hong et al. 2006) is used for the boundary layer parameterization, and the Grell-Devenyi cumulus scheme (Grell and Devenyi 2002) is used for the cumulus parameterization, but only in the outer two domains (at 45 km and 15 km grid spacings). In addition, the Dudhia (Dudhia 1989) and rapid radiative transfer model (Mlawer et al. 1997) schemes are used for short and longwave radiation, respectively.

Table 1. Dimensions, grid spaces, and time steps for model domains in Ernesto simulations

Domain	Dimension (x × y × z)	Grid space	Time step
1	125 × 70 × 36	45 km	120 s
2	331 × 148 × 36	15 km	40 s
3	844 × 340 × 36	5 km	13.3 s

Table 2. Dimensions, grid spaces, and time steps for model domains in Nuri simulations

Domain	Dimension (x × y × z)	Grid space	Time step
1	182 x 112 × 36	45 km	120 s
2	361 x 202 × 36	15 km	40 s
3	772 x 412 × 36	5 km	13.3 s

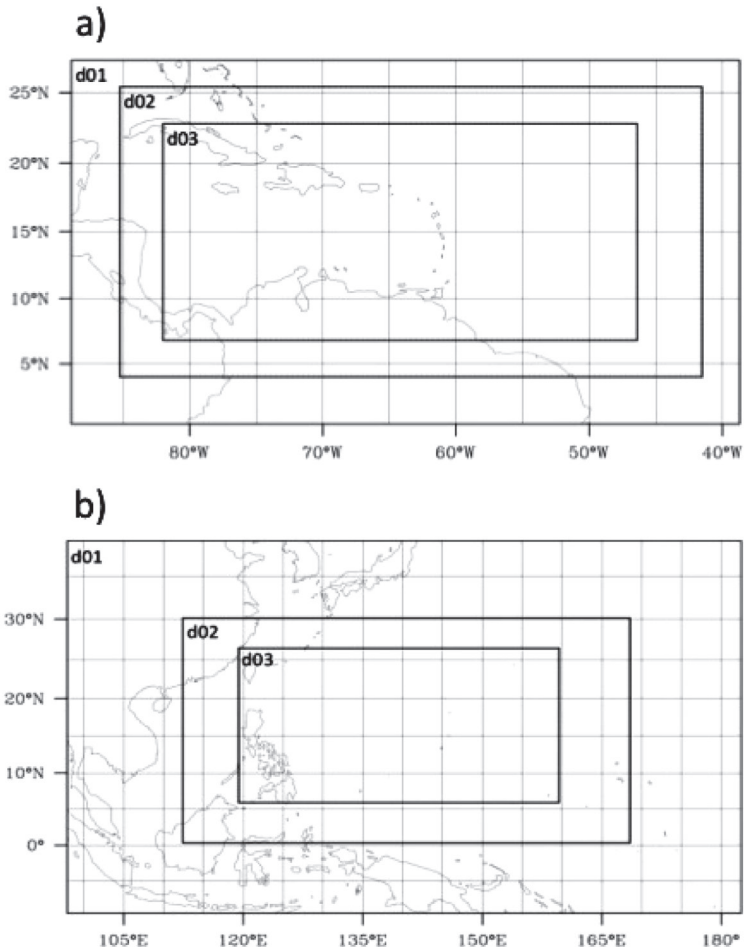

FIG. 1. The locations of WRF domains used for ensemble simulations of Hurricane Ernesto (a) and Typhoon Nuri (b).

d. Numerical experiments: Ensemble forecasts with SKEBS

Following Cheung and Elsberry (2002) and Snyder et al. (2010), we define the genesis time for Hurricane Ernesto as occurring when the NHC designated it a tropical depression at 1800 UTC 24 August 2006. In order to predict the genesis of Ernesto, the forecast initial time is set at 0000 UTC 24 August 2006 and the ensemble simulations last 18 h, until 1800 UTC 24 August 2006. This abbreviated period is due to the computational cost of WRF with SKEBS.

The control ensemble forecast (CNTL, hereafter) is a set of regional ensemble forecasts using WRF, generated by initial conditions (ICs) derived from the NCEP Global Ensemble Forecast System (GEFS), and boundary conditions (BCs) derived from NCEP Global Forecast System (GFS) 1x1° final analysis (FNL) data. Although the initial perturbations in the CNTL are not directly generated for WRF, it still represents a compatible set of regional high-resolution ensemble forecasts, as shown in an earlier study (Thatcher and Pu 2013). Considering that GEFS has only 14 members in 2006 and also considering the computational cost of high-resolution ensemble forecasts, the WRF regional ensemble experiments with SKEBS will use 14 members to achieve consistent comparisons with the CNTL.

The SKEBS method influences the forecast through potential temperature (θ) and streamfunction forcings, whose amplitudes can be specified in the WRF namelist input file (Berner et al. 2011). One may also specify whether a constant or random phase structure of the vertical pattern generator is desired, and whether the SKEBS option should affect each of the domains individually.

For the ensemble forecasts with SKEBS, the backscatter option was turned on for each of the three domains in the initial conditions, but not for the boundary conditions. Preliminary tests were conducted to determine the proper values of dissipation rate specification at the time of integration. We found that the values of 2.0 E-6 m^2m^{-3} for θ dissipation and 1.0 E-5 m^2m^{-3} for streamfunction dissipation produce simulations that predict Ernesto's genesis without producing any spurious artifacts. Therefore, the following

experiments will carefully delineate the dissipation values by varying them from these values (referred to as "defaults" hereafter). Note that the default value for potential temperature dissipation is 1.0 E-6 m^2m^{-3} in the recent WRF release, when the tests were done for midlatitude synoptic cases. Considering the higher amount of convection and cumulus parameterization-based energy dissipation in the tropics compared to that in the midlatitudes, our default value of 2.0 E-6 m^2m^{-3} can be physically justified. In addition, by default, the random vertical pattern generator was turned off in the SKEBS experiments.

Table 3 lists the ensemble experiments with SKEBS. Note that the control (BS_CNTL) uses the default values specified above with 14 members. Unless otherwise specified, the default values remain the same through the following experiments. To test the impact of the random vertical pattern generator, BS_VERT is conducted with the generator turned on. The BS_THHALF ensemble uses a dissipation rate of 1.0 E-6 m^2m^{-3} to test the individual effects of the parameter on the resulting forecasts of TC genesis. Overall, the computational time for each of the SKEBS ensembles is about three or four times that for the CNTL.

A SKEBS ensemble forecast (BS_CNTL_NURI) is also conducted for Typhoon Nuri (2008), with the simulation beginning 18 h before genesis at 0000 UTC 16 August 2008. This simulation uses the same default dissipation rates and physics parameterizations as those specified for Ernesto's ensemble experiments. The corresponding domain setup is specified in Table 2 and Figure 1.

3. Basic evaluation of ensemble forecasts of TC genesis with SKEBS

a. Ensemble biases over time

As a first examination of the results of the various backscatter ensemble forecasts, the bias of water vapor and θ is calculated over time (Figure 2). Bias here represents the ensemble mean, in terms of the variable being discussed, minus the corresponding analysis field, expressed as

$$\frac{1}{n}\sum_{k=1}^{n}(\bar{f}_k - a_k) \tag{1}$$

where $\bar{f}_k$ denotes the ensemble mean of forecasts across the 14 ensemble members, a denotes the analysis, k denotes the grid points across the domain, and n is the total grid points in the model domain. The analysis field uses the NCEP FNL analysis and is interpolated into the WRF model domains.

TABLE 3. Configuration of ensemble forecasts with SKEBS

Ensemble experiments	Th Amplitude	Psi Amplitude	Vertically random
BS_CNTL	2E-6	1E-5	Off
BS_VERT	2E-6	1E-5	On
BS_THHALF	1E-6	1E-5	Off
BS_CNTL_NURI	2E-6	1E-5	Off

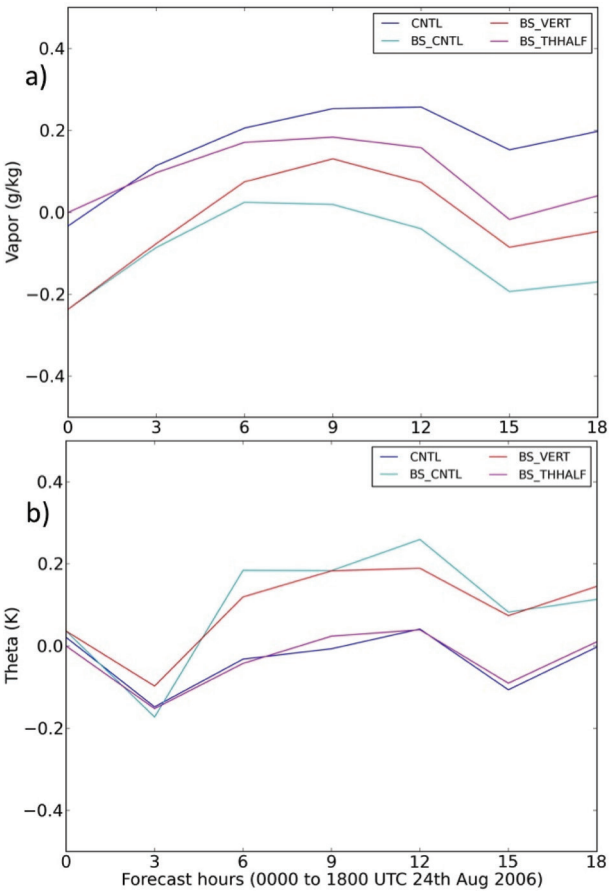

FIG. 2. Time series of bias for a) vapor (g kg^{-1}) and b) potential temperature (theta; unit: K) at 850 hPa for different ensemble experiments with SKEBS, compared with CNTL.

Charron et al. (2010) found that backscatter schemes occasionally made ensemble bias worse. We first checked the time evolution of biases at various pressure levels over the simulation period. Overall the biases were small for both water vapor and potential temperature and similar for other variables, although the variation with height was quite notable. As an example, Figure 2 shows the biases at 850 hPa for both water vapor and potential temperature (theta or θ) in various ensemble experiments. The ensemble forecasts with the default parameters of SKEBS (BS_CNTL) produce a unique bias profile compared to the CNTL (without SKEBS), while the other experiments with SKEBS fall in between. In order to check the statistical significance of the differences between the CNTL and BS_CNTL bias, we use the Kolmogorov-Smirnov two-sample test and find that for vapor (θ) there is a 0.4 (2.8) % chance that the two come from the same distribution. In other words, the correspond-

ing p-values fall well below a 5% alpha threshold for both vapor and θ. Thus, it appears that at the TC- and latent heating-critical height of 850 hPa, the SKEBS default provides the most helpful counterpoint to initial condition–based (CNTL) ensemble forecasts.

To better understand the bias differences by height, Figure 3 shows the averaged bias between 1200 and 1800 UTC 24 August 2006 (12 to 18 h simulation). It appears that the θ bias (Figure 3a), confirming what Charron et al. (2010) found, is quite large in all the SKEBS forecasts compared with the CNTL, except perhaps for the BS_THHALF. This occurs most clearly from 925 hPa up to 600 hPa. For water vapor (Figure 3b), the results are roughly reversed. In most of the SKEBS ensemble forecasts, the water vapor bias is less than that in the CNTL up to around 600 hPa. Among the various SKEBS settings, the BS_CNTL and BS_VERT generally show the least bias for both vapor and θ above 700 hPa, which confirms that default dissipation rates of 2.0 E-6 and 1.0 E-5 m^2/m^3 for the temperature and streamfunction, respectively, are reasonable in the tropics.

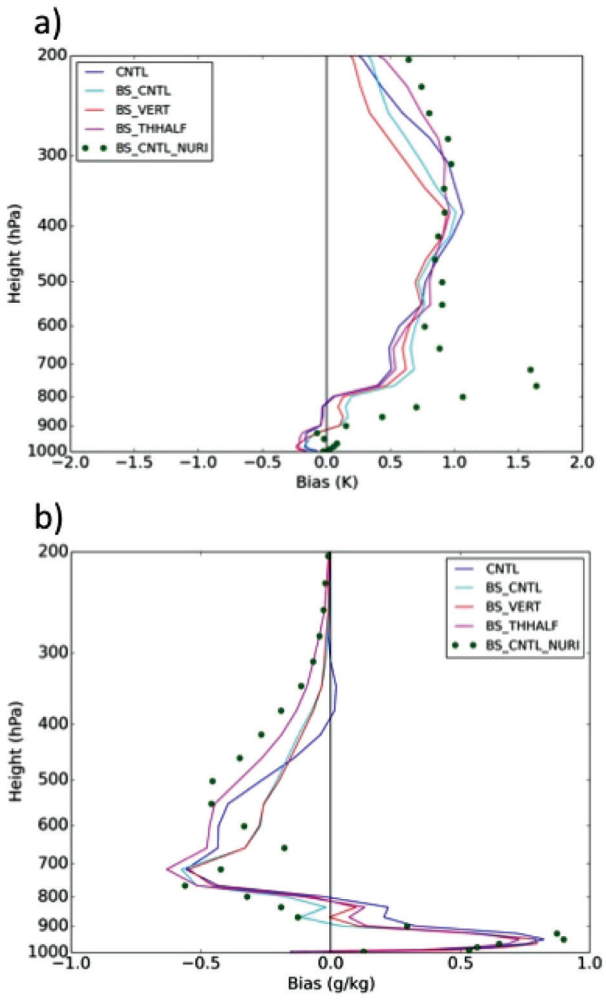

FIG. 3. Variation of the biases with heights averaged over 12 to 18 h simulations for ensemble experiments. a) theta (K) b) vapor (g kg^{-1}).

The bias of Nuri's ensemble forecasts with SKEBS is significantly higher than that of Ernesto. It generally produces much more vapor below 850 hPa and too little moisture above (Figure 3a), and much more heating at almost all levels (Figure 3b), but especially at lower levels. Since there is no control ensemble forecast for Nuri available for comparison, the differences between Ernesto and Nuri show only case-by-case variability.

b. Probability of TC genesis

The probability of SKEBS ensemble forecasts producing Ernesto's genesis is first evaluated and the results are compared with those from the CNTL. As mentioned above, following Cheung and Elsberry (2002) and Snyder et al. (2010), we define the genesis time as occurring when the National Hurricane Center (NHC) and the Joint Typhoon Warning Center (JTWC) designated Ernesto and Nuri as tropical depressions at 1800 UTC 24 August 2006 and 1800 UTC 16 August 2008, respectively. In order to determine whether TC genesis occurs in a certain member of an ensemble forecast, a closed isobar must be present in the sea level pressure field. There must be a closed 850 hPa geopotential contour of 1496 m or below and a vorticity maximum, both of which must be found within, or overlap, a closed wind circulation at 850 hPa. This set of criteria was derived from downscaled global analyses at the WRF model resolution used in this study, and also considering the fact that the "genesis" should preserve the system to be developed as tropical storm or cyclone later. To be clear, for genesis to be counted as occurring at 1800 UTC 24 August 2006 for Ernesto or 1800 UTC 18 August 2008 for Nuri, these characteristics must be present at those times.

Figure 4 shows geopotential height, vorticity, and wind vectors at 850 hPa for each member in the control ensemble forecast (CNTL) at 1800 UTC 24 August 2006. It is apparent that forecast disturbances are quite intense in several members at this time, although tropical depressions are typically quite weak, with a wind minimum of only 33 knots. Despite the intense circulations seen in members 4, 5, and 7, there is also a notable ensemble spread. For instance, the disturbances in member 3 are comparatively unorganized.

To compare how the near-TC genesis region responds to varying effects of backscatter methods, and also to examine the overall ability of the SKEBS ensembles to predict TC genesis (comparable to Figure 4), Figures 5–7 show the outcomes from BS_CNTL, BS_VERT, and BS_THHALF. Specifically, in BS_CNTL (Figure 5), there is significant variability between the members in terms of disturbance strength, especially in terms of geopotential height. Note that the vorticity variability is notably smaller in the ensemble forecasts with SKEBS compared with the CNTL. This may relate to the namelist parameter setting for stream-

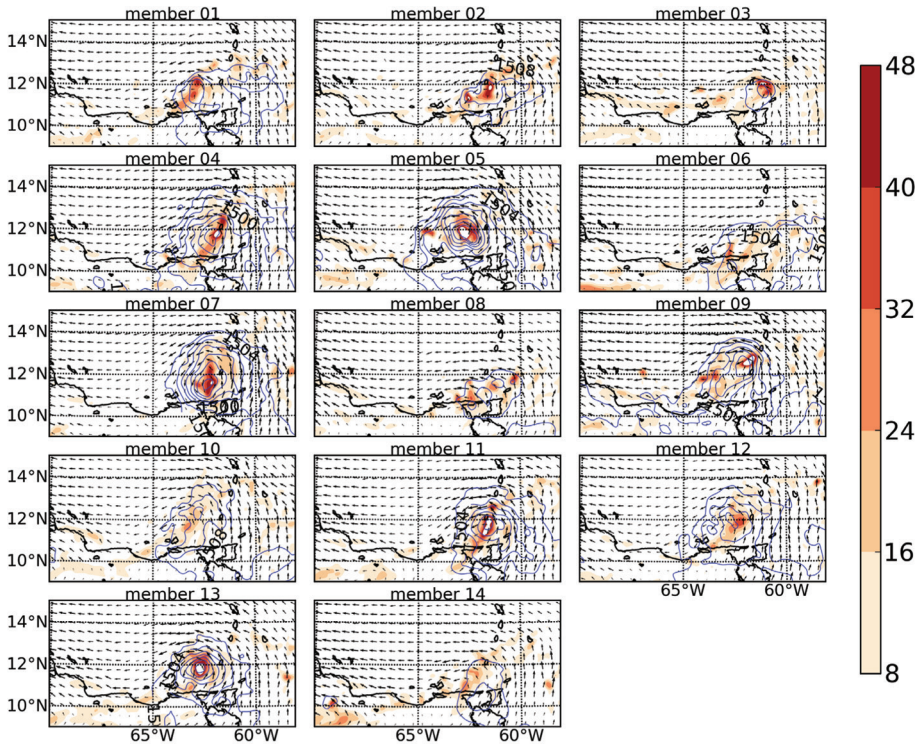

FIG. 4. Vorticity (shaded; * 10^{-5} s^{-1}) and geopotential height (contours; 4 m intervals) of CNTL ensemble members at 850 hPa at 1800 UTC 24 2006.

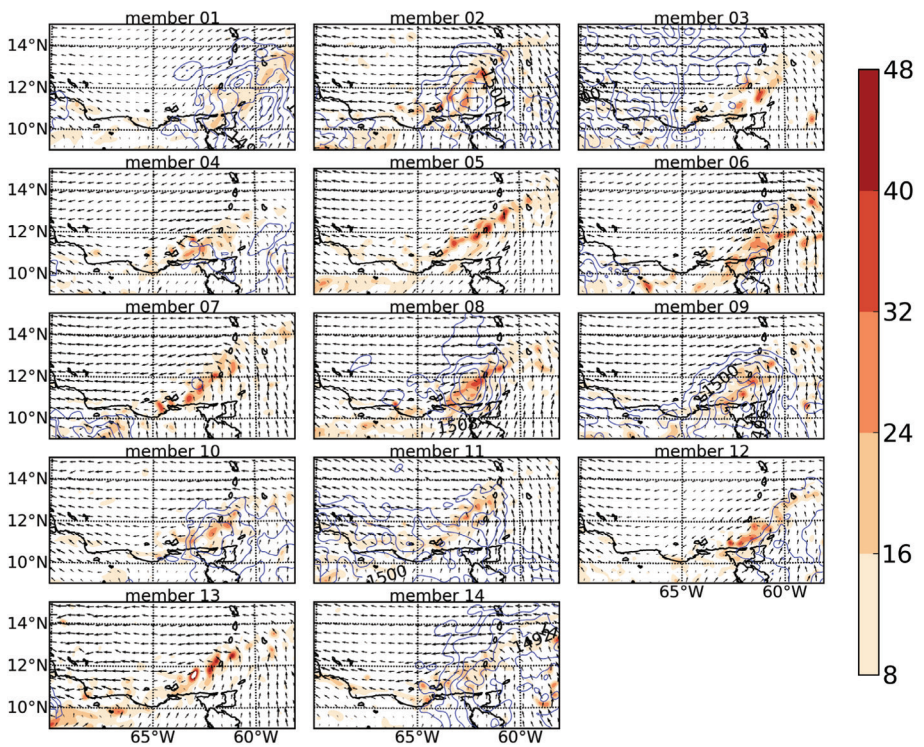

FIG. 5. Vorticity (shaded; * 10^{-5} s^{-1}) and geopotential height (contours; 4 m intervals) of BS_CNTL ensemble members at 850 hPa at 1800 UTC 24 August 2006.

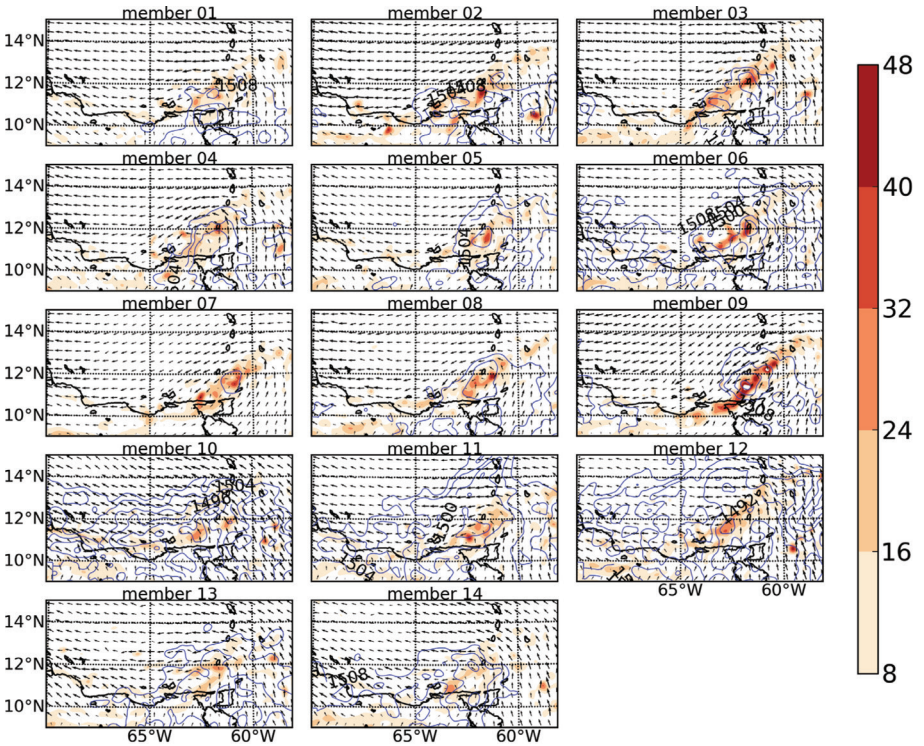

FIG. 6. Vorticity (shaded; * 10^{-5} s^{-1}) and geopotential height (contours; 4 m intervals) of BS_VERT ensemble members at 850 hPa at 1800 UTC 24 August 2006.

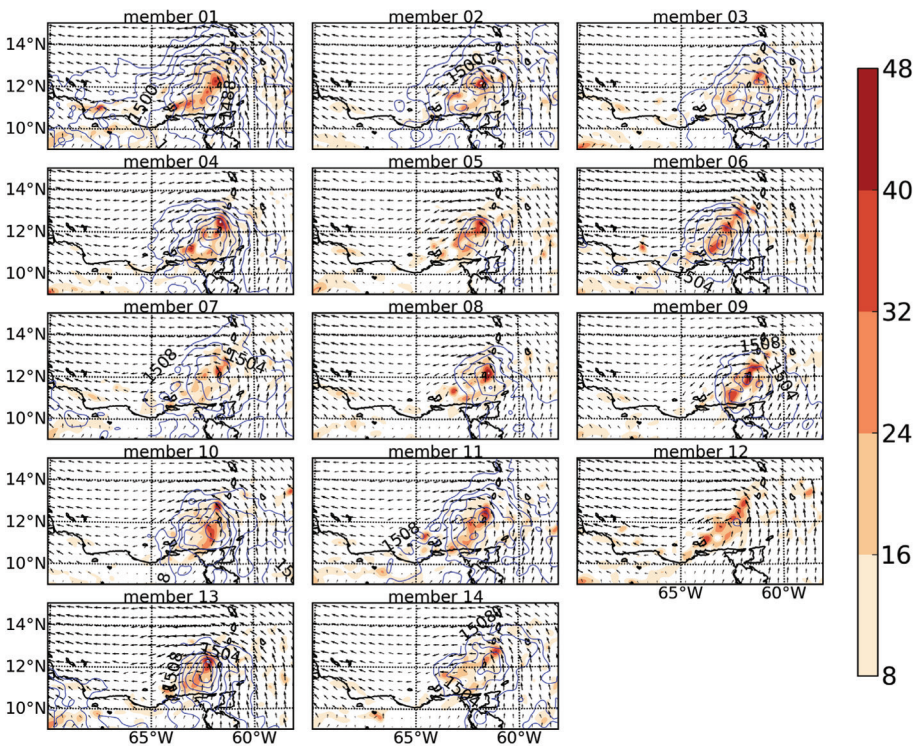

FIG. 7. Vorticity (shaded; * 10^{-5} s^{-1}) and geopotential height (contours; 4 m intervals) of BS_THHALF ensemble members at 850 hPa at 1800 UTC 24 August 2006.

function dissipation in SKEBS. Overall, the BS_CNTL produces notably less intense disturbances than the CNTL does. As a result, the CNTL shows 7 out of 14 ensemble members predicting the genesis, whereas the BS_CNTL ensemble has a genesis rate of 4 out of 14 (Table 4). In addition, the geographically extended geopotential height anomalies throughout the domain in members 3 and 14 in the BS_CNTL (Figure 5) appear nonphysical compared with any of the members in the CNTL ensemble (Figure 4). These unique geopotential height patterns may be related to the fact that SKEBS is adding energy in terms of θ, which is closely related to geopotential height, and do not appear to coincide with nonphysical features in other fields.

Comparing SKEBS ensemble forecasts with (BS_VERT; Figure 6) and without (BS_CNTL, Figure 5) a random phase vertical pattern generator, we find that both have members that predict TC genesis as well as members whose disturbances are more similar to ordinary easterly waves; both ensembles have 4 out of 14 members exhibiting TC genesis (Table 4). A similar result for BS_THHALF is illustrated in Figure 7. Here the temperature perturbations and geopotential height minima are much more collocated with the vorticity maxima compared to the other SKEBS ensembles. While the spread in vorticity maxima for the BS_THHALF is similar to that of the BS_CNTL, the vorticity positioning patterns are notably different between the two. While BS_CNTL ensemble members show a fairly consistent southwest to northeast alignment in terms of the vorticity maxima, this pattern is not present after halving the temperature dissipation in BS_THHALF. Largely due to the more coherent geopotential height structures, the BS_THHALF ensemble shows 11 out of 14 members predicting genesis, which is the highest of all ensemble forecasts with SKEBS. While BS_THHALF does produce better-organized disturbances, we again find that there is reduced intensity spread among the members compared with the BS_CNTL ensemble. However, while the BS_CNTL ensemble (Figure 5) shows several members (4, 7, 12, 13) without a closed circulation, concentrated vorticity, or a notable geopotential height drop and several members with fairly intense disturbances (2, 8, 9), the BS_THHALF ensemble (Figure 7) does not produce a forecast without a closed circulation and notable vorticity.

To analyze the SKEBS ensemble forecast characteristics in a different case, we examine the control backscatter parameters in a forecast of Typhoon Nuri (2008). Figure 8 shows synoptic views for each member of Nuri's ensemble forecast at its observed genesis time (1800 UTC 16 August 2008). Significant variability in spatial disturbances as well as in their intensity is found across the ensemble members. The ensemble members in BS_CNTL_NURI show notably higher intermember vorticity variability than that in Ernesto's BS_CNTL, despite the fact that the same dissipation rates are used in both experiments. In addition, the members of Nuri's ensemble forecast show much more variability in the circulation structure. For example, in member 2 (Figure 8) a wave is barely visible, while in member 5 an easterly wave with a vorticity maximum is quite notable; member 8 shows a closed circulation with an 850 hPa vorticity maximum and a nearby geopotential height minimum; and member 10 displays a well-organized TC with an intense closed circulation, a strong (collocated) vorticity maximum, and a geopotential height drop of ~16 m more than that in member 8. Overall, Ernesto's BS_CNTL (Figure 5) provides very dissimilar intermember vorticity patterns compared to BS_CNTL_NURI, which shows the dependency of the intra-ensemble SKEBS results on the particular case.

Considering the difficulty of forecasting Nuri, as found in a previous study (Snyder et al. 2011), the well-organized forecasts of Nuri in members 6, 7, 8, 10, and 11 (Figure 8), and the accompanying organization spread in BS_CNTL_NURI, it appears that the backscatter settings can produce ensemble forecasts with the ability both to predict TC genesis in difficult environments and to provide a notable spread to indicate the large accompanying uncertainty. This is highlighted by comparison with a WRF deterministic run, which is shown in Figure 9. In addition, since the deterministic forecast (Figure 9) using WRF with NCEP FNL initial and boundary conditions fails to predict Nuri's genesis, and 8 out of 14 ensemble members with SKEBS do predict Nuri's genesis, ensemble forecasting with SKEBS is greatly advantageous and shows promise in terms of predicting TC genesis.

Table 4. Genesis statistics in various ensemble-forecasting experiments

Ensemble experiments	Genesis rate
CNTL	07/14
BS_CNTL	04/14
BS_VERT	04/14
BS_THHALF	11/14
BS_CNTL_NURI	08/14

4. Characteristics of error growth and underdispersion of ensemble forecasts

The above results show that ensemble forecasts produced by SKEBS have the ability to produce forecasts of TC genesis. At the same time, however, Berner et al. (2009) averred that nearly all ensembles are underdispersive, which motivated their work on SKEBS. It naturally follows that underdispersion would be a primary metric to evaluate the ensemble forecasts with SKEBS as compared to the CNTL. In this section, we examine underdispersion in TC genesis environments.

a. Early simulation period: Pre-genesis phase

To examine how the model error–based SKEBS ensem-

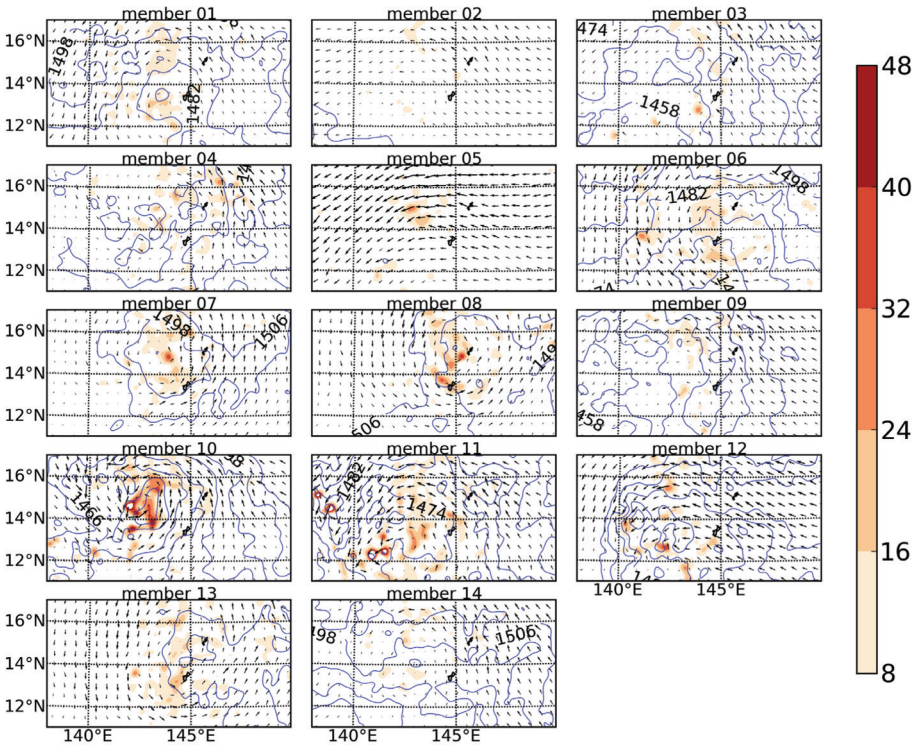

FIG. 8. Vorticity (shaded; * 10^{-5} s^{-1}) and geopotential height (contours; 4 m intervals) of BS_CNTL_NURI ensemble members at 850 hPa at 1800 UTC 16 August 2008.

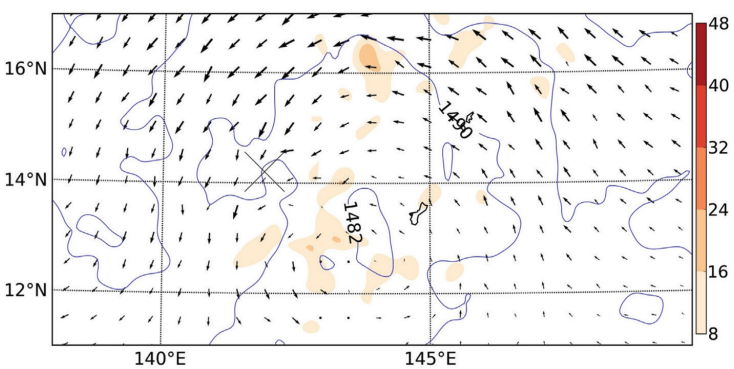

FIG. 9. Vorticity (shaded; * 10^{-5} s^{-1}) and geopotential height (contours; 4 m intervals) of Hurricane Nuri at 850 hPa at 1800 UTC 16 August 2008 from WRF deterministic forecast using FNL initial and boundary conditions.

ble dispersion develops and evolves relative to that of the initial condition error–based CNTL ensemble forecasts at various wavelengths, a spectral analysis of both ensemble perturbations and errors (ensemble forecast versus NCEP FNL analysis) is conducted using a Fast-Fourier Transform (FFT) calculation in the meridional direction.

Figure 10 shows results averaged zonally for all ensemble members for 850 geopotential heights at 0300, 0600, and 0900 UTC 24 August 2008 for Ernesto. It is apparent that there is significant underdispersion during the first 9 h in all the forecasts, including the CNTL, as the perturbations (solid lines) are consistently lower than the error (dotted lines). In addition, the underdispersion is worse at large wavelengths than it is at small wavelengths, and it slowly decreases over the 9 h period. At 0300 UTC the CNTL displays a much steeper perturbation slope than the BS_CNTL does, and it thus appears that, much more so than the SKEBS ensembles, the initial perturbations used in the CNTL are first created on a large scale. Correspondingly, after only 3 h of simulation (Figure 10a), the perturbations

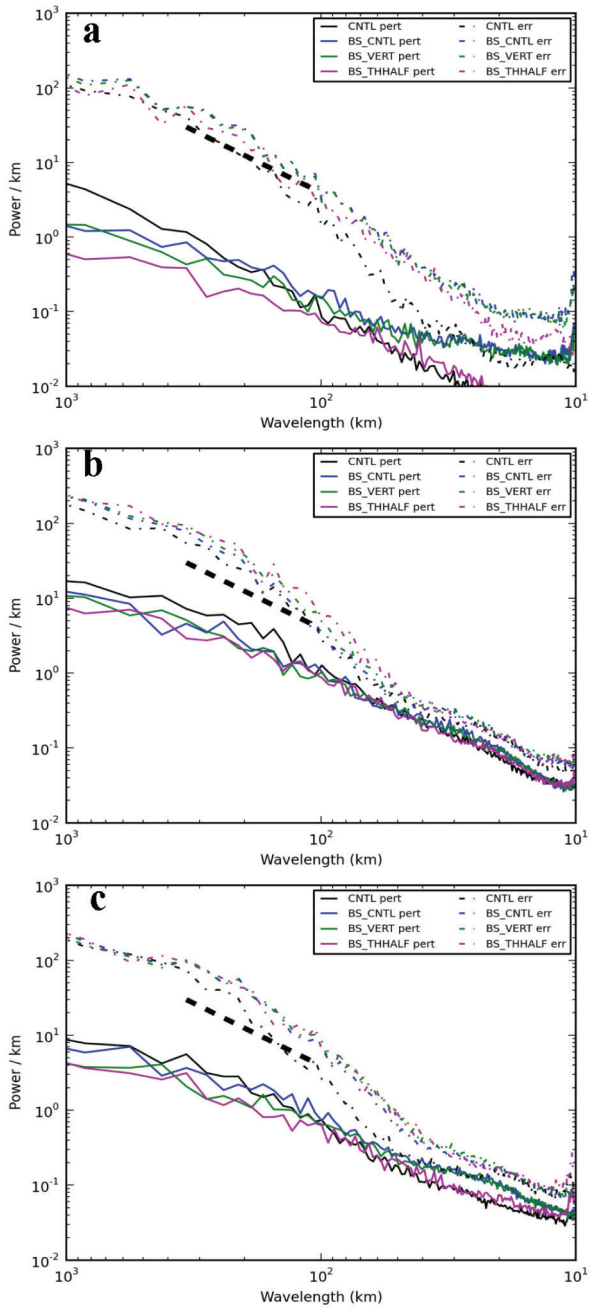

FIG. 10. Fast Fourier Transform-based spectral analysis of 850 hPa geopotential height perturbations and errors across a zonal and ensemble average for the Ernesto ensembles at a) 0300 UTC, b) 0600 UTC, and c) 0900 UTC 24th August. The bold dash line denotes the slope of $k^{-5/3}$.

at wavelengths smaller than 100 km are larger for the BS_CNTL and BS_VERT than they are for the CNTL. Overall, these results accurately characterize the nature of the energy backscatter. By 0600 UTC the slopes of the BS_CNTL and BS_VERT perturbations have notably steepened compared to the CNTL and BS_THHALF ensembles, perhaps as BS_THHALF is particularly affected as the energy added on a small scale is transported upscale. By 0900 UTC, the perturbations below 100 km wavelength for all SKEBS ensembles are quite similar, and it is in this part of the spectrum that we find the smallest underdispersion for all ensembles.

The same calculation is performed for the u component of the wind at 850 hPa (Figure 11) over the first 9 h of the simulation. We find that the error and perturbation slopes are notably steeper below 100 km of wavelength for all ensembles at 0300 UTC, compared to the corresponding slopes at the 850 hPa geopotential height. This is especially true in BS_CNTL and BS_VERT. This u versus geopotential height slope difference may imply that the u field displays an upscale transfer of energy faster than does the geopotential height field. By 0300 UTC, when we double the backscattered temperature rate (BS_CNTL versus BS_THHALF), we find that BS_CNTL demonstrates less underdispersion in the related geopotential height (Figure 10a), but this difference between BS_CNTL and BS_THHALF disappears by 0900 UTC.

b. Midsimulation period: Near the TC genesis phase

To better compare spectral perturbation and error differences between ensemble configurations, we average the FFT calculations not only over the ensemble members and in a zonal direction across the entire domain, but also from 1200 to 1800 UTC for geopotential height (Figure 12a) and the u component of the wind (Figure 12b) at 850 hPa. Overall, for both geopotential height and u, we find that the underdispersion reaches a minimum around 50-60 km wavelength. The underdispersion differences among different ensemble configurations for geopotential height are quite minimal. Above 100 km wavelength, the CNTL ensemble shows slightly less underdispersion than the ensemble forecasts with SKEBS. In terms of the u component of the wind at 850 hPa, the ensemble underdispersion with SKEBS is generally not any less than that of the CNTL. In addition, the backscatter dissipation rate for temperature (BS_THHALF) and the vertical random pattern generator (BS_VERT) do not create notable differences from BS_CNTL.

To examine the underdispersion near the TC environment, Figure 13 shows dispersion spectra similar to those in Figure 12, but averaged within a box measuing 1000 km per side, centered on the simulated pre-Ernesto centers. This provides us with data on how well SKEBS and CNTL ensembles create perturbations that match the associated error in TC-proximate environments. The noticeable difference in this TC-proximate area, compared with the domain-wide ensemble spatial spectra, is that the underdispersion decreases consistently. This underdispersion decrease occurs for all ensembles, at most wavelengths, and whether

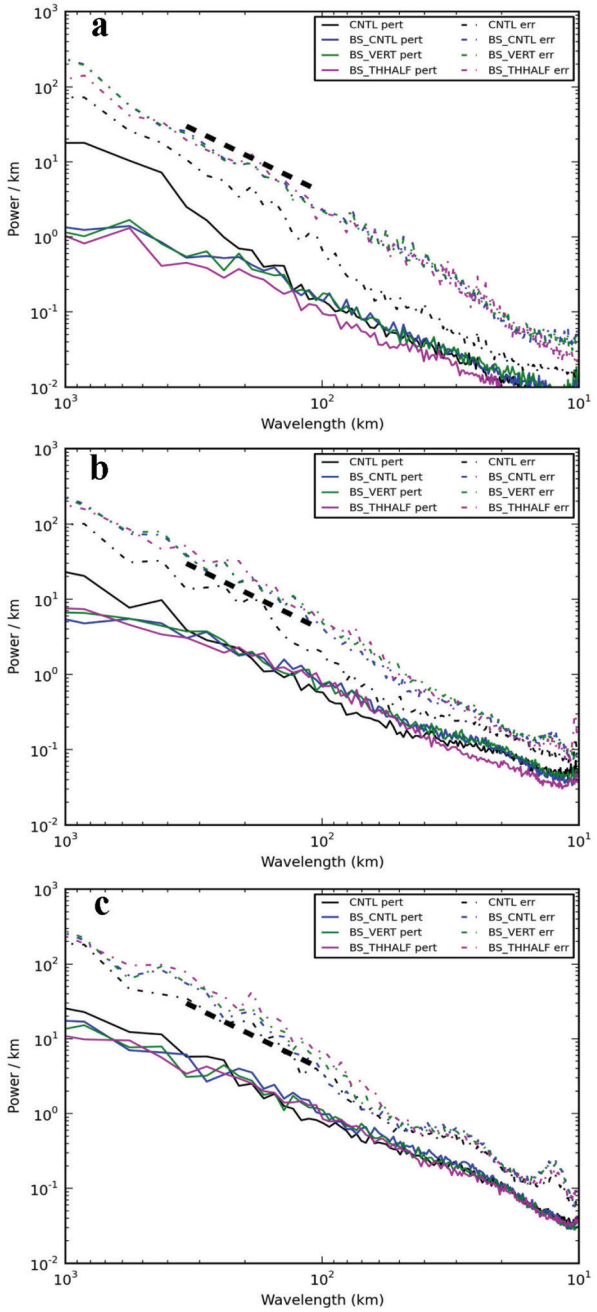

FIG. 11. Fast Fourier Transform-based spectral analysis of 850 hPa u perturbations and errors across a zonal and ensemble average for Ernesto ensembles at a) 0300 UTC, b) 0600 UTC, and c) 0900 UTC 24th August. The bold dash line denotes the slope of $k^{-5/3}$.

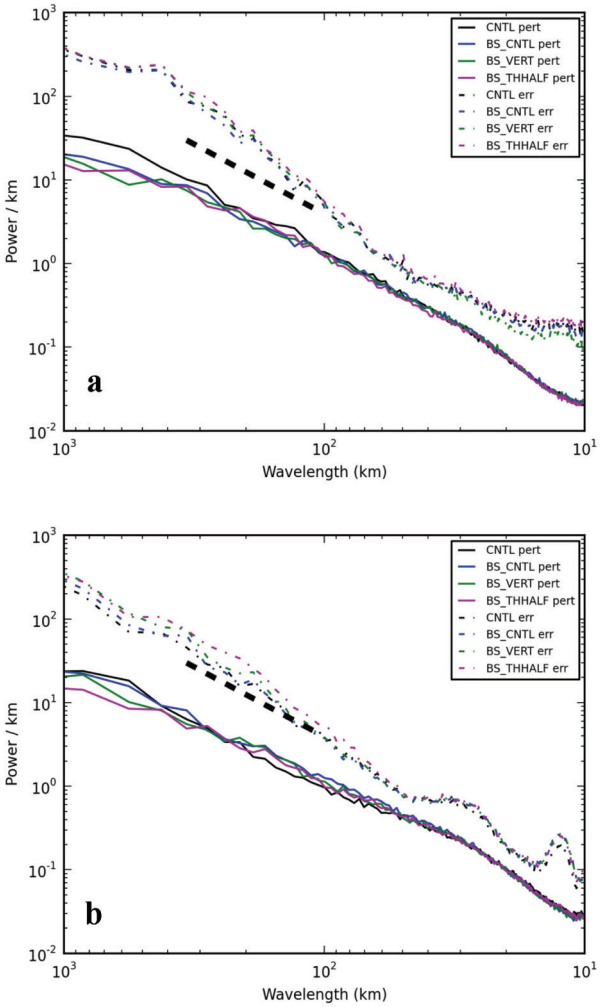

FIG. 12. Fast Fourier Transform-based spectral analysis of 850 hPa perturbations and errors across a zonal and ensemble average from 1200-1800 UTC 24th over entire model domain (d03 in Figure 1a) for a) geopotential height and b) u wind component. The bold dash line denotes the slope of $k^{-5/3}$.

one examines the geopotential or u fields. The decreases in underdispersion may imply that ensemble forecasting with SKEBS and GEFS-based ensembles are both skillful at predicting uncertainty in the TC-proximate environment.

To further compare TC-proximate values to those over the TC core, we again calculate 850 hPa geopotential and u dispersion spectra, but now average within a box measuring only 200 km per side, centered on the TC (Figure 14). Note that the energy spectra are quite different from those in Figures 13 and 14, which is partially due to the smaller spectral domain, such that comparisons between TC-proximate and TC core underdispersion have to be made carefully. Within this TC core area, the CNTL ensemble shows less underdispersion than the SKEBS ensembles, primarily in terms of the u component of the wind. Across the spectrum, for u, we find that the CNTL ensemble provides notably large perturbation sizes and relatively low error. Of the SKEBS ensembles, we find that BS_CNTL is lowest in terms of the u component error. Changes to the random vertical pattern generator and temperature dissipation rate do

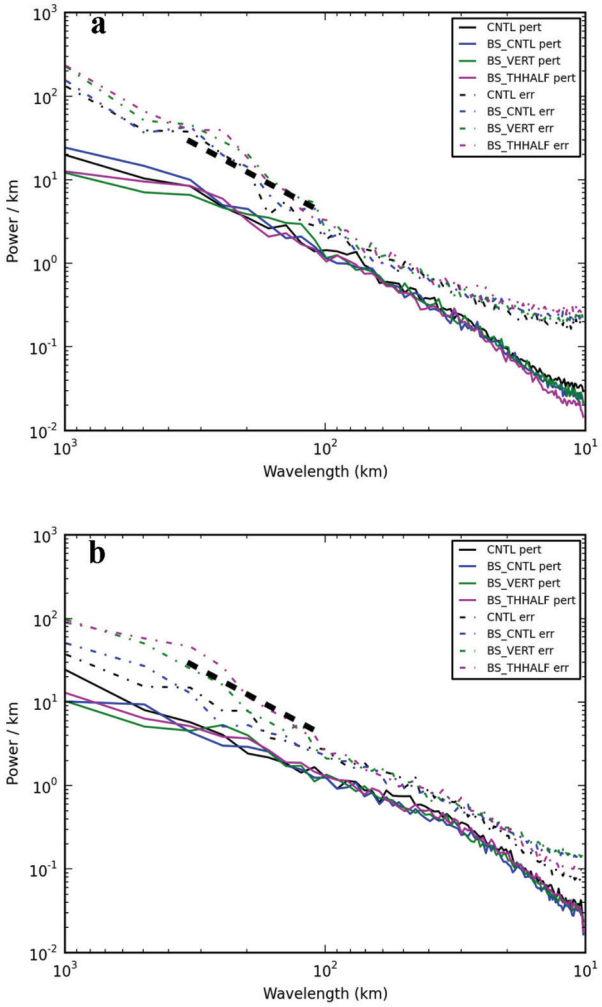

Fig. 13. Same as Figure 12, except the calculations within a 1000-km-per-side box, centered on the simulated TC instead of the entire domain. The bold dash line denotes the slope of $k^{-5/3}$.

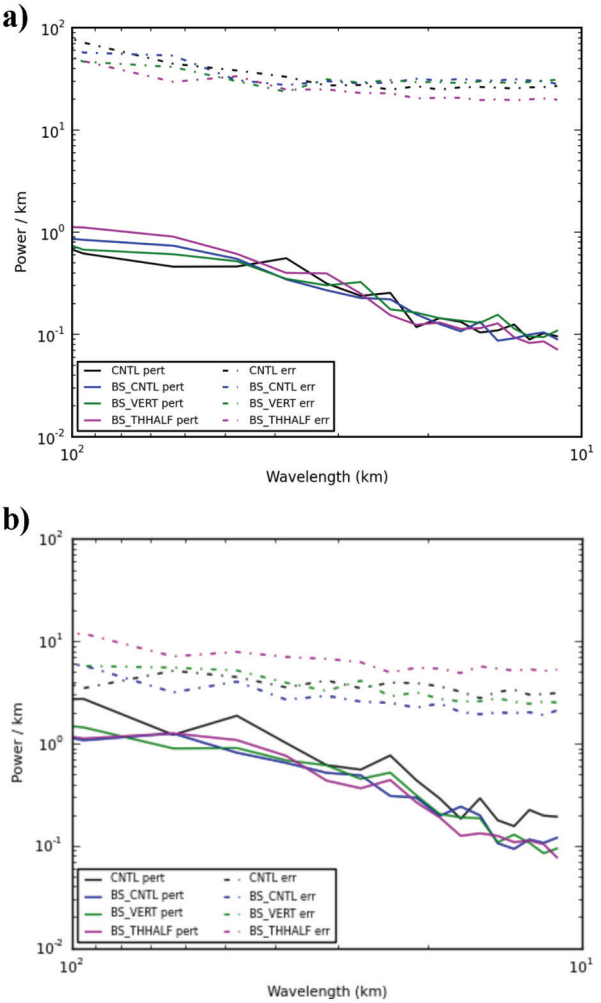

Fig. 14. Similar to Figure 13, except the calculations within a 200-km-per-side box, centered on the simulated TC.

not appear to lead to notable changes in geopotential error or perturbation energy spectra. Overall, these results imply that the added computational costs of SKEBS may not be justified in light of its relatively mediocre underdispersion characteristics.

5. Conclusions

In order to evaluate the SKEBS ensemble forecasts in terms of TC genesis predictability and also to characterize the accompanying ensemble underdispersion, in this study we created various ensemble forecasts using the WRF model with SKEBS at 5 km horizontal resolution to predict the genesis of Hurricane Ernesto (2006). Ensemble forecasts with SKEBS are compared against a control ensemble forecast with the WRF model using initial conditions derived from NCEP GEFS. A similar ensemble forecast with SKEBS, 18 h ahead of the genesis of Typhoon Nuri, is also conducted. Compared to previous studies with ensemble forecasts using SKEBS at grid spacings of at least 40 km (e.g., Berner et al. 2009, 2011, 2012), this study represents one of the first evaluations of the SKEBS method in high-resolution ensemble forecasts.

We found that SKEBS ensemble forecasts have potential to generate realistic probabilistic forecasts for TC genesis. Specifically, whereas the deterministic forecast fails to predict the genesis of Typhoon Nuri, the ensemble forecast produced by SKEBS is able to predict genesis in 8 out of 14 total ensemble members. Of the various configurations of SKEBS ensemble forecasts of Hurricane Ernesto, all of these reproduce Ernesto's genesis to some degree.

A spectral analysis of both ensemble perturbations and errors (ensemble forecast versus NCEP FNL analysis) is conducted using a Fast-Fourier Transform (FFT) calcula-

tion in the meridional direction to examine how the SKEBS ensemble dispersion develops and evolves relative to that of the initial condition perturbation–based CNTL ensemble forecasts at various wavelengths. It is found that after only 3 h of simulation, the perturbations at wavelengths smaller than 100 km are already larger for the BS_CNTL than they are for the initial condition–based CNTL. By 6 h the BS_CNTL and BS_VERT ensemble perturbation spectral slopes have notably steepened as the energy added primarily on a small scale is transported upscale.

The spectral patterns at 1200–1800 UTC for both geopotential height and u at 850 hPa over the entire model domain show the least underdispersion around 50–60 km wavelength. At this time, the CNTL shows slightly less underdispersion than the various SKEBS ensemble forecasts for both geopotential height and the u component of wind. In addition, we find that changing the temperature dissipation rate and turning on the vertical random pattern generator do not create notably different dispersion profiles compared to BS_CNTL over the model domain.

Within a 1000km × 1000km box centered on the simulated TCs, we find that underdispersion decreases for all ensembles at most wavelengths for 850 hPa u and geopotential heights. This implies that ensemble forecasts do a better job of matching perturbation sizes to errors at the same wavelengths in TC-proximate regions, compared to the background tropics. In the TC core region, the CNTL ensemble (without SKEBS) provides relatively low error and high dispersion, and thus the lowest underdispersion, of all ensembles. These results may imply that the initial perturbation–based ensemble forecast is more skillful in providing dispersion characteristics within the inner-core structures of tropical cyclones, and using only SKEBS may not be adequate for generating reasonable TC inner core forecasts.

The results of this study show the potential of using SKEBS ensemble forecasts in TC genesis forecasts. However, in terms of both realistic physical spread and underdisperion characteristics, the downscaled GEFS-based ensemble produces better forecasts. In addition, in this study, we use only 14 ensemble members owing to the consideration of computational expenses and available CNTL ensemble forecasts. The limited number of ensemble members may be one reason for the notable underdispersion of the ensembles discussed. Future work should emphasize more case studies, a larger ensemble size, various forecast leading times, and more sophisticated high-resolution analysis and initial condition perturbation–based ensemble forecasts in order to accurately assess the forecast errors and obtain more robust conclusions.

Acknowledgments

The authors greatly appreciate the NCAR WRF model development group for their efforts in developing the community model. We also thank the Center for High Performance Computing (CHPC) at the University of Utah for their computing support. This study is supported by a research grant from the Office of Naval Research (ONR) through award numbers N000141310582.

References

Berner, J., M. L. G. Shutts, and T. Palmer, 2009: A spectral stochastic kinetic energy backscatter scheme and its impact on flan dependent predictability in the ECMWF ensemble prediction system. *J. Atmos. Sci*., **66,** 603–626.

----, S.-Y. Ha, J. P. Hacker, A. Fournier, and C. Snyder, 2011: Model uncertainty in a mesoscale ensemble prediction system: Stochastic versus multiphysics representations. *Mon. Wea. Rev.,* **139,** 1972–1995.

----, T. Jung, and T. N. Palmer, 2012: Systematic model error: The impact of increased horizontal resolution versus improved stochastic and deterministic parameterizations. *J. Climate,* **25,** 4946–4962.

Buizza, R., 1997: Potential forecast skill of ensemble prediction and spread and skill distributions of the ECMWF ensemble prediction system. *Mon. Wea. Rev.,* **125,** 99–119.

Charron, M., G. Pellerin, L. Spacek, P. L. Houtekamer, N. Gagnon, H. L. Mitchell, and L. Michelin, 2010: Toward random sampling of model error in the Canadian Ensemble Prediction System. *Mon. Wea. Rev.,* **138,** 1877–1901.

Chen, S.-H., and W.-Y. Sun, 2002: A one-dimensional time dependent cloud model. *J. Meteor. Soc. Japan*, **80,** 99–118.

Cheung, K. K. W., and R. L. Elsberry, 2002: Tropical cyclone formations over the western north Pacific in the Navy Operational Global Atmospheric Prediction System forecasts. *Wea. Forecasting,* **17,** 800–820.

Dudhia, J., 1989: Numerical study of convection observed during the Winter Monsoon Experiment using a mesoscale two-dimensional model. *J. Atmos. Sci.*, **46,** 3077–3107.

Fritsch, J. M., J. Hilliker, J. Ross, and R. L. Vislocky, 2000. Model consensus. *Wea. Forecasting,* **15,** 571–582.

Grell, G. A., and D. Devenyi, 2002: A generalized approach to parameterizing convection combining ensemble and data assimilation techniques. *Geoph. Res. Lett.,* **29**, 10.1029/2002GL015311, 2002.

Hagedorn, R., F. J. Doblas-Reyes, and T. N. Palmer, 2005: The rationale behind the success of multi-model ensembles in seasonal forecasting—I. Basic concept. *Tellus*, **57A,** 219–233.

Hong, S. Y., Y. Noh, and J. Dudhia, 2006: A new vertical diffusion package with an explicit treatment of entrainment processes. *Mon. Wea. Rev*., **134,** 2318–2341.

Houtekamer, P. L., L. Lefaivre, J. Derome, H. Ritchie, and H. L. Mitchell, 1996: A system simulation approach to ensemble prediction. *Mon. Wea. Rev.,* **124,** 1225–1242.

Li, X., M. Charron, L. Spacek, and G. Candille, 2008: A regional ensemble prediction system based on moist targeted singular vectors and stochastic parameter perturbations. *Mon. Wea. Rev*., **136,** 443–462.

Liu, H., J. Anderson, and Y.-H. Kuo, 2012: Improved analyses and forecasts of Hurricane Ernesto's genesis using radio occultation data in an ensemble filter assimilation system. *Mon. Wea. Rev.,* **140,** 151–166.

Mlawer, E. J., S. J. Taubman, P. D. Brown, M. J. Iacono, and S. A. Clough, 1997: Radiative transfer for inhomogeneous atmosphere: RRTM, a validated correlated-k model for the longwave. *J. Geophys. Res.,* **102,** 16 663–16 682.

Nastrom, G. D., and K. S. Gage, 1985: A climatology of atmospheric wavenumber spectra of wind and temperature observed by commercial aircraft. *J. Atmos. Sci.,* **42,** 950–960.

Reynolds, C. A., J. Teixeira, and J. G. McLay, 2008: Impact of

stochastic convection on the ensemble transform. *Mon. Wea. Rev.,* **136,** 4517–4526.

Shutts, G. J., 2005: A kinetic energy backscatter algorithm for use in ensemble prediction systems. *Quart. J. Roy. Meteor. Soc.,* **131,** 3079–3102.

Skammarock, W. C., J. B. Klemp, J. Dudhia, D. O. Gill, D. M. Barker, M. G. Duda, X.-Y. Huang, W. Wang, and J. G. Powers, 2008: A description of the Advanced Research WRF Version 3. NCAR Tech. Note NCAR/TN-475+STR., June 2008, 133 pp.

Snyder, A., Z. Pu, and Y. Zhu, 2010: Tracking and verification of the east Atlantic tropical cyclone genesis in NCEP global ensemble: Case studies during NASA African monsoon multidisciplinary analyses. *Wea. Forecasting*, **25,** 1397–1411.

----, Z. Pu, and C.A. Reynolds, 2011: Impact of stochastic convection on ensemble forecasts of tropical cyclone development. *Mon. Wea. Rev.,* **139,** 620–626.

Teixeira, L., and C. A. Reynolds, 2008: Stochastic nature of physical parameterizations in ensemble prediction: A stochastic convection approach. *Mon. Wea. Rev*., **136,** 483–496.

Thatcher, L., and Z. Pu, 2013: Evaluation of tropical cyclone genesis precursors with relative operating characteristics (ROC) in high-resolution ensemble forecasts: Hurricane Ernesto. *Tropical Cyclone Research and Review*, **2,** 131–148.

Toth, Z., and E. Kalnay, 1993: Ensemble forecasting at NMC: The generation of perturbations. *Bull. Amer. Meteor. Soc.,* **74,** 2317– 2330.

----, and E. Kalnay, 1997: Ensemble forecasting at NCEP and the breeding method. *Mon. Wea. Rev.,* **125,** 3297–3319.

Wei, M., Z. Toth, R. Wobus, Y. Zhu, and C. H. Bishop 2006: Initial perturbations based on the ensemble transform (ET) technique in the NCEP global ensemble forecast system. NOAA/NCEP Office Note 453, 33 pp.